RMetS
Royal Meteorological Society

Modelling of local length-scale dynamics and isotropizing deformations

O. Pannekoucke,[a,b]* E. Emili[a] and O. Thual[a,c]

[a]*CERFACS/CNRS URA 1875, Toulouse, France*
[b]*CNRM/GAME, Météo-France/CNRS UMR 3589, Toulouse, France*
[c]*Université de Toulouse, INPT, CNRS, IMFT, Toulouse, France*

*Correspondence to: Olivier Pannekoucke, CERFACS/PAE, 42 Av. G. Coriolis, 31057 Toulouse Cedex, France.
E-mail: olivier.pannekoucke@cerfacs.fr

The correlation length-scale which characterizes the shape of the correlation function is often used to parametrize correlation models. This article describes how the length-scale dynamics can be employed to estimate a spatial deformation (coordinate transformation). Of particular interest is the isotropizing deformation, which transforms anisotropic correlation functions into quasi-isotropic ones. The evolution of the length-scale field under a simple advection dynamics is described in terms of the local metric tensor. This description leads to a quadratic constraint satisfied by the isotropizing deformation and from which a system of Poisson-like partial differential equations is deduced. The isotropizing deformation is obtained as the solution of a coupled system of Poisson-like partial differential equations. This system is then solved with a pseudo-diffusion scheme, where the isotropizing deformation is the steady-state solution. The isotropization process is illustrated within a simulated 2D setting. The method is shown to provide an accurate estimation of the original deformation used to build the anisotropic correlations in this idealized framework.

Applications in data assimilation are discussed. First, the isotropization procedure can be useful for background-error covariance modelling. Secondly, the length-scale dynamics provides a way to simulate the dynamics of covariances for the transport of passive scalars, as encountered in chemical data assimilation.

Key Words: length-scale dynamics; covariance modelling; deformation; isotropization

Received 6 September 2012; Revised 23 May 2013; Accepted 23 May 2013; Published online in Wiley Online Library 9 October 2013

1. Introduction

Data assimilation aims to provide an analysis state, $\mathbf{x}^{\mathrm{a}}$, that is a realistic representation of the state of the atmosphere $\mathbf{x}^{\mathrm{t}}$ at a given time. This analysis $\mathbf{x}^{\mathrm{a}}$ is constructed as a background state $\mathbf{x}^{\mathrm{b}}$ corrected by information due to observations $\mathbf{y}^{\mathrm{o}}$. In the variational formulation, the analysis is obtained as the minimum of the cost function

$$\begin{aligned} J(\mathbf{x}) =& (\mathbf{x}-\mathbf{x}^{\mathrm{b}})^{\mathrm{T}}\mathbf{B}^{-1}(\mathbf{x}-\mathbf{x}^{\mathrm{b}}) \\ &+ (\mathbf{y}^{\mathrm{o}}-\mathbf{H}\mathbf{x})^{\mathrm{T}}\mathbf{R}^{-1}(\mathbf{y}^{\mathrm{o}}-\mathbf{H}\mathbf{x}), \end{aligned} \tag{1}$$

where $\mathbf{B}=\mathbb{E}[\boldsymbol{\epsilon}^{\mathrm{b}}\boldsymbol{\epsilon}^{\mathrm{b}\mathrm{T}}]$ denotes the covariance matrix of the background error $\boldsymbol{\epsilon}^{\mathrm{b}}=\mathbf{x}^{\mathrm{b}}-\mathbf{x}^{\mathrm{t}}$, $\mathbf{R}=\mathbb{E}[\boldsymbol{\epsilon}^{\mathrm{o}}\boldsymbol{\epsilon}^{\mathrm{o}\mathrm{T}}]$ denotes the covariance matrix of the observational error $\boldsymbol{\epsilon}^{\mathrm{o}}=\mathbf{y}^{\mathrm{o}}-\mathbf{H}\mathbf{x}^{\mathrm{t}}$, and $\mathbf{H}$ is the linearized observation operator that maps the model state to observation locations. The $\mathbf{B}$ Matrix is often expanded as $\mathbf{B}=\boldsymbol{\Sigma}\mathbf{C}\boldsymbol{\Sigma}^{\mathrm{T}}$ where $\boldsymbol{\Sigma}$ is a diagonal matrix filled with the standard deviations of background error (i.e. the square root of the diagonal elements of $\mathbf{B}$) and $\mathbf{C}=\boldsymbol{\Sigma}^{-1}\mathbf{B}\boldsymbol{\Sigma}^{-\mathrm{T}}$ is a correlation matrix.

A correlation matrix is the discrete representation of a field of correlation functions $\rho(\mathbf{x},\mathbf{y})$. These correlation functions depend on each other; if one function is modified, then all other functions should also be modified in order to conserve the symmetry and the positiveness that define correlation functions.

Correlation functions are said to be homogeneous in the case where there exists a translation invariance so that $\rho(\mathbf{x},\mathbf{y})=\rho(\mathbf{x}-\mathbf{y})$ (on the plane, but the equivalent exists with the rotation on the sphere). The correlations are said to be isotropic when $\rho(\mathbf{x},\mathbf{y})=\rho(|\mathbf{x}-\mathbf{y}|)$. Note that isotropy implies homogeneity, but the reverse depends on the domain. There exist domains, e.g. the plane and the bi-periodic domain, where correlations can be homogeneous without being isotropic. However, on the sphere, homogeneity is equivalent to isotropy (Gaspari and Cohn, 1999): two homogeneous anisotropic correlations transported from two separated points on the Equator toward the North Pole would lead to different correlations at this point, which contradicts the homogeneity assumption, while the two correlations would be the same under the isotropy assumption.

The $\mathbf{B}$ matrix is a key component of data assimilation systems and depends on the dynamics (Bouttier, 1993) and the analysis

cycles (Bouttier, 1994). Under the perfect model assumption and linear dynamics, the dynamics of the $\mathbf{B}$ matrix is provided by the forecast step of the Kalman filter (Kalman, 1960), and is given by $\mathbf{B} = \mathbf{M}\mathbf{A}\mathbf{M}^{\mathrm{T}}$ where $\mathbf{A} = \mathbb{E}[\boldsymbol{\epsilon}^{\mathrm{a}}\boldsymbol{\epsilon}^{\mathrm{a}\mathrm{T}}]$ denotes the covariance matrix of analysis error $\boldsymbol{\epsilon}^{\mathrm{a}} = \mathbf{x}^{\mathrm{a}} - \mathbf{x}^{\mathrm{t}}$, $\mathbf{M}$ is the linear propagator and $\mathbf{M}^{\mathrm{T}}$ its adjoint. Yet this propagation of information is computationally expensive and cannot be applied in practice. Since the publication of Ezensen (1994), ensemble methods offer an attractive way to propagate the statistics at a lower cost.

However, due to the small sample size, the ensemble covariance matrix is rank deficient, and possibly imbalanced (Kepert, 2009; Greybush *et al.*, 2011), so that the associated sampling noise needs to be filtered out, usually with a localization procedure that involves a Schur product (Houtekamer and Mitchell, 2001) with a compactly supported correlation function. Even with the increase of computer power, the increasing complexity of numerical weather prediction systems still limits the use of large ensembles. This is particularly true for convection-resolving systems that require high resolution associated with fine-scale description of physical processes.

Hence, many efforts have been made in order to mimic the covariance time evolution and to better represent important features of spatial covariance functions. Commonly used covariance models include for instance the spectral diagonal assumption, which models homogeneous correlations (Courtier *et al.*, 1998), the wavelet diagonal assumption (Fisher, 2003), recursive filters (Purser *et al.*, 2003) or spatial deformations (coordinate transformation) (Desroziers, 1997; Michel, 2013a,b).

In particular, the spatial deformation method is quite attractive since it provides an inexpensive method to construct anisotropic correlation from the deformation of an isotropic correlation (for which efficient parallelized implementation exists). However the problem remains of estimating, from economical diagnosis, the coordinate system in which the statistics are isotropic.

An economical diagnosis of the local shape of correlation functions is provided by the correlation length-scale. This is the length over which the correlation remains significant. In data assimilation, when the second derivative of the correlation function exists, assuming the correlation function $\rho(x, y)$ is flat at points $x = y$, the one-dimensional length-scale as defined by Daley (1991) is given by

$$L(x) = \sqrt{\frac{1}{-\partial_y^2 \rho(x,y)|_{y=0}}}. \tag{2}$$

It can also be described from the local metric tensor $(\mathbf{g}_{\mathbf{x}})_{ij} = -\partial^2_{ij}\rho$ defined from the Taylor expansion of the local correlation, assuming that $\rho(\mathbf{x})$ is differentiable and flat at the origin

$$\rho(\mathbf{x}, \mathbf{x} + \delta\mathbf{x}) \underset{\mathbf{x}}{\approx} 1 - \frac{1}{2}||\delta\mathbf{x}||^2_{\mathbf{g}_{\mathbf{x}}} + \mathcal{O}(\delta\mathbf{x}^3),$$

where $||\mathbf{x}||^2_{\mathbf{E}} = \mathbf{x}^{\mathrm{T}}\mathbf{E}\mathbf{x}$. The local metric tensor $\mathbf{g}_{\mathbf{x}}$ is related to the local length-scales along x^i according to $L_i = 1/\sqrt{g_{ii}}$, where $g_{ij} = (\mathbf{g}_{\mathbf{x}})_{ij}$. In 2D,

$$\mathbf{g}_{\mathbf{x}} = \begin{pmatrix} \dfrac{1}{L_x^2(\mathbf{x})} & \dfrac{1}{L_{xy}(\mathbf{x})} \\ \dfrac{1}{L_{xy}(\mathbf{x})} & \dfrac{1}{L_y^2(\mathbf{x})} \end{pmatrix},$$

where $L_x(\mathbf{x})$ and $L_y(\mathbf{x})$ are the one-dimensional length-scales along the x and y directions.

The local metric is thus related to the local correlation by

$$||\delta\mathbf{x}||^2_{\mathbf{g}_{\mathbf{x}}} = f[\rho(\mathbf{x}, \mathbf{x} + \delta\mathbf{x})] + \mathcal{O}(|\delta\mathbf{x}|^3), \tag{3}$$

where the function $f(r) = 2(1 - r)$ follows from the local parabola-based assumption (Pannekoucke *et al.*, 2008), but other forms for f can be used (Pannekoucke *et al.*, 2008). Note that the assumption made of a flat correlation at the origin lays aside some classes of correlation function, e.g. the exponential correlation (First-Order Auto Regressive) $\rho(\mathbf{x}, \mathbf{x} + \delta\mathbf{x}) = \mathrm{e}^{-||\delta\mathbf{x}||_{\mathbf{g}_{\mathbf{x}}}}$. But since all the information we need in this article is encoded in the metric $\mathbf{g}_{\mathbf{x}}$, this kind of correlation functions can be also used with an appropriate choice of f in Eq. (3).

In addition to describing the local correlation shape, the length-scales (or the metric tensor $\mathbf{g}_{\mathbf{x}}$) can be used to tune correlation models. For instance, in the diffusion-based covariance model proposed by Weaver and Courtier (2001), Pannekoucke and Massart (2008) demonstrated how to objectively fix the diffusion tensor $\nu_{\mathbf{x}}$ from the ensemble estimation of the local metric $\mathbf{g}_{\mathbf{x}}$ according to $\mathbf{g}_{\mathbf{x}}^{-1} = 2\nu_{\mathbf{x}}$. As shown in Massart *et al.* (2012), this calibration based upon the length-scale diagnosis has a positive impact on analysis.

The dynamics of forecast-error covariances has been detailed by Cohn (1993) who provides explicit partial differential equations (PDEs) for the evolution of the forecast-error variance and correlation length-scale. This approach has been used by Menard *et al.* (2000) who have implemented a full Kalman filter with an explicit time evolution of the bulk covariance functions, with appropriate correction of the variance field. A similar approach has been employed by Lyster *et al.* (2004) under a fully Lagrangian implementation.

The present contribution is focused on the use of the length-scale dynamics, in the simplified version of a pure transport without model error, to solve the problem of isotropization. The work is detailed as follows.

Section 2 describes the effect of a spatial deformation on the local length-scales. This leads, in section 3, to a way to estimate an isotropizing deformation from the local length-scales. These theoretical elements are then supported by numerical experiments in a 2D setting, detailed in section 4. Applications in data assimilation are then described in section 5. Finally, conclusions are detailed in section 6.

2. Dynamics of length-scales and isotropization

2.1. Deformation of background-error correlations

The idea behind correlation modelling based on isotropizing deformations is that a relatively complicated correlation model (anisotropic) can be obtained from a spatial deformation of a simpler one (Desroziers, 1997). It is generally convenient to consider a change of variable $\widetilde{\mathbf{x}} = D(\mathbf{x}) = \mathbf{x} + d(\mathbf{x})$ so that an anisotropic correlation ρ_D in the deformed coordinate system can be deduced from a homogeneous one ρ_{h} by a relation of the form

$$\rho_D(\widetilde{\mathbf{x}}, \widetilde{\mathbf{y}}) = \rho_{\mathrm{h}}[D^{-1}(\widetilde{\mathbf{x}}), D^{-1}(\widetilde{\mathbf{y}})], \tag{4}$$

where the reciprocal deformation $D^{-1}(\widetilde{\mathbf{x}}) = \widetilde{\mathbf{x}} + \widetilde{d}(\widetilde{\mathbf{x}})$ using a semi-Lagrangian method from the inverse displacement $-\delta = \widetilde{d}(\widetilde{\mathbf{x}})$, solution of the fixed-point equation

$$\delta = d[\widetilde{\mathbf{x}} - \delta]. \tag{5}$$

With this approach, it is thus possible to create sharp correlation functions in the vicinity of front structures for instance (Desroziers, 1997).

One can also note that the deformation process is similar to the advection of a passive scalar under the effect of a wind field $\mathbf{u}$

$$\frac{\mathrm{d}\alpha}{\mathrm{d}t} = \partial_t\alpha + \mathbf{u}\cdot\nabla\alpha = S(\alpha), \tag{6}$$

for which the deformation $D(\mathbf{x}) = \mathbf{x} + \mathbf{u}(\mathbf{x})\mathrm{d}t$ is introduced to integrate over $\mathrm{d}t$. Here, $S(\alpha)$ denotes the sink/source term. For

linear S, like a diffusion $S(\alpha) = \Delta\alpha$, the error $\boldsymbol{\epsilon}^{\mathrm{b}}$ affecting the estimation of α follows the same dynamics

$$\frac{\mathrm{d}\boldsymbol{\epsilon}^{\mathrm{b}}}{\mathrm{d}t} = \partial_t \boldsymbol{\epsilon}^{\mathrm{b}} + \mathbf{u}\cdot\nabla\boldsymbol{\epsilon}^{\mathrm{b}} = S(\boldsymbol{\epsilon}^{\mathrm{b}}), \tag{7}$$

establishing a bridge between the dynamics of error and the covariance modelization based on deformations. The effect of a spatial deformation on the local length-scales is detailed below for the particular conservative case ($S(\alpha) = 0$).

2.2. Transformation of length-scales

Under the action of a deformation $D(\mathbf{x}) = \widetilde{\mathbf{x}}$, where $\widetilde{\mathbf{x}}$ denotes the local coordinate in the new coordinate system, the correlation functions ρ are transformed into the correlation functions ρ_D according to

$$\rho_D(\widetilde{\mathbf{x}}, \widetilde{\mathbf{x}} + \delta\widetilde{\mathbf{x}}) = \rho\left[D^{-1}(\widetilde{\mathbf{x}}), D^{-1}(\widetilde{\mathbf{x}} + \delta\widetilde{\mathbf{x}})\right]. \tag{8}$$

The equivalent of Eq. (3) in the new coordinate system is

$$||\delta\widetilde{\mathbf{x}}||^2_{\widetilde{\mathbf{g}}_{\widetilde{\mathbf{x}}}} = f\big[\rho_D(\widetilde{\mathbf{x}}, \widetilde{\mathbf{x}} + \delta\widetilde{\mathbf{x}})\big] + \mathcal{O}(|\delta\widetilde{\mathbf{x}}|^3), \tag{9}$$

where the local tensor $\widetilde{\mathbf{g}}_{\widetilde{\mathbf{x}}}$ can be deduced from the local tensor field $\mathbf{g}_{\mathbf{x}}$, as detailed in Appendix A, so that

$$\widetilde{\mathbf{g}}_{\widetilde{\mathbf{x}}} = (\mathbf{D}^{-1}_{\widetilde{\mathbf{x}}})^{\mathrm{T}}\mathbf{g}_{D^{-1}(\widetilde{\mathbf{x}})}\mathbf{D}^{-1}_{\widetilde{\mathbf{x}}}. \tag{10}$$

We obtain here a key result: the local shape of the deformed correlations is completely governed by the transformation of local tensors $\mathbf{g}_{\mathbf{x}}$ by the Jacobian of the deformation.

2.3. Deformation of isotropic correlations and isotropization

As a particular case, one can describe the action of the deformation on isotropic correlations in flat space, defined by a single correlation length-scale L_{h}, such that for all positions $\mathbf{x}$,

$$\mathbf{g}_{\mathbf{x}} = L_{\mathrm{h}}^{-2}\,\mathbf{I}, \tag{11}$$

where $\mathbf{I}$ is the identity matrix.

The local tensor $\widetilde{\mathbf{g}}_{\widetilde{\mathbf{x}}}$ resulting from the action of a deformation D on these isotropic correlations is given by

$$\widetilde{\mathbf{g}}_{\widetilde{\mathbf{x}}} = L_{\mathrm{h}}^{-2}(\mathbf{D}^{-1}_{\widetilde{\mathbf{x}}})^{\mathrm{T}}\mathbf{D}^{-1}_{\widetilde{\mathbf{x}}}. \tag{12}$$

Under the hypothesis of isotropic correlations, local features of the deformed correlations are thus completely governed by the local dilation tensor $(\mathbf{D}^{-1}_{\widetilde{\mathbf{x}}})^{\mathrm{T}}\mathbf{D}^{-1}_{\widetilde{\mathbf{x}}}$ of the inverse deformation.

In the next section, it is shown how to invert this procedure in order to find a deformation that transforms anisotropic correlations into isotropic ones.

2.4. Isotropization of anisotropic correlations

The important contribution provided by the two previous sections is that the local features of the deformed correlations are completely determined by the dilation tensor associated with the inverse deformation. This suggests that one could use this relation in order to deduce the deformation that has led to a given tensor field $\mathbf{g}_{\widetilde{\mathbf{x}}}$ (estimated in practice from an ensemble; Belo Pereira and Berre, 2006; Pannekoucke and Massart, 2008).

The isotropization is the procedure that aims to provide a particular deformation $\overset{\circ}{D}$ so that its action on general heterogenous correlations ρ produces isotropic correlations $\rho_{\overset{\circ}{D}} = \rho_{\mathrm{h}}$. In the new coordinate system, the local metric is thus $\widetilde{\mathbf{g}}_{\widetilde{\mathbf{x}}} = \widetilde{L}_{\mathrm{h}}^{-2}\mathbf{I}$, where $\mathbf{I}$ denotes the identity matrix and $\widetilde{L}_{\mathrm{h}}$ is a length-scale, unknown for the moment. From the one-to-one mapping between $\mathbf{x}$ and $\widetilde{\mathbf{x}}$, Eq. (10) can be written as

$$(\overset{\circ}{\mathbf{D}}_{\mathbf{x}})^{\mathrm{T}}\,\overset{\circ}{\mathbf{D}}_{\mathbf{x}} = \widetilde{L}_{\mathrm{h}}^{2}\,\mathbf{g}_{\mathbf{x}}. \tag{13}$$

This equation directly links the isotropizing deformation with the local length-scales through the metric tensor $\mathbf{g}_{\mathbf{x}}$.

In the particular case where the correlation functions result from the deformation by D of an isotropic correlation function, $\overset{\circ}{D}$ is no more than the inverse deformation D^{-1}.

To estimate an isotropization deformation, Michel (2013a,b) has proposed a procedure that relies on a wavelet estimation of the gradient of deformation (Clerc and Mallat, 2002).

In the present contribution, the approach we develop relies on the local metric tensor, which is relatively easy to estimate in practice (Belo Pereira and Berre, 2006; Pannekoucke *et al.*, 2008; Pannekoucke and Massart, 2008).

3. Estimation of deformation from local length-scales

3.1. Discussion on the quadratic constraint

In the 1D case, the equivalent of Eq. (13) when assuming that $\partial_x D$ is positive is

$$\partial_x \overset{\circ}{D}(x) = \frac{\widetilde{L}_{\mathrm{h}}}{L(x)}, \tag{14}$$

where $L(x)$ is the diagnosed length-scale field estimated from the data (ensemble method or transport). While the unknown length-scale $\widetilde{L}_{\mathrm{h}}$ is present in this relation, it can be dropped as follows. The second-order derivative of D is

$$\partial_x^2 \overset{\circ}{D}(x) = -\frac{\widetilde{L}_{\mathrm{h}}}{L^2(x)}\partial_x L,$$

where by definition of the derivative of $\overset{\circ}{D}$ (Eq. (14)), the quotient $\widetilde{L}_{\mathrm{h}}/L(x)$ can be replaced by $\partial_x \overset{\circ}{D}$, leading to the Poisson-like equation

$$\partial_x^2 \overset{\circ}{D} = \left(-\frac{1}{L}\partial_x L\right)\partial_x \overset{\circ}{D}, \tag{15}$$

where $\widetilde{L}_h$ has gone. Note that the defect of this equation is that it implies a discontinuous coordinate transformation for periodic domains. This can be avoided considering the equivalent equation in terms of displacement field $\overset{\circ}{D}(x) = x + \overset{\circ}{d}(x)$, with

$$\partial_x^2 \overset{\circ}{d} = \left(-\frac{1}{L}\partial_x L\right)\left(1 + \partial_x \overset{\circ}{d}\right), \tag{16}$$

where the solution $\overset{\circ}{d}$ is periodic.

In the 2D case, it would be convenient to have an equivalent method to deduce the isotropization deformation. In particular, the problem would be easy to solve if it was possible to deduce the Jacobian matrix $\overset{\circ}{\mathbf{D}}_{\mathbf{x}}$ from Eq. (13). In that case, a Helmholtz decomposition would lead to two classical Poisson PDE: one for the curl and one for the divergent part of the displacements.

However, there is no unique solution for equations like Eq. (13): any matrix $\mathbf{O}\mathbf{g}_{\mathbf{x}}^{1/2}$, with $\mathbf{O}$ an orthogonal matrix (that is $\mathbf{O}^{\mathrm{T}} = \mathbf{O}^{-1}$) and $\mathbf{g}_{\mathbf{x}}^{1/2}$ a square-root of $\mathbf{g}_{\mathbf{x}}$ (obtained from the singular vector decomposition or with the Choleski decomposition), is also a solution of Eq. (13). Thus the problem remains of how to smoothly connect deformations from one point to another one; this is now addressed.

3.2. General formalism for the isotropization procedure

From the formalism of differential geometry (Feynman *et al.*, 2002; Nakahara, 2003; Zdunkowski and Bott, 2003; Ciarlet, 2006) Eq. (10) is written as

$$g_{ij} = \partial_{x^i} \widetilde{x}^\alpha \, \partial_{x^j} \widetilde{x}^\beta \, \widetilde{g}_{\alpha\beta} \,, \tag{17}$$

where x^i ($\widetilde{x}^\alpha$) denotes the ith (αth) component of the coordinate system $\mathbf{x}$ ($\widetilde{\mathbf{x}}$). The derivatives of the metric g_{ij} along x^k

$$\partial_{x^k} g_{ij} = \Gamma_{kij} + \Gamma_{kji}, \tag{18}$$

introduce the Christoffel symbols of the first kind defined by $\Gamma_{ijk} = \left(\partial_{x^i} g_{jk} + \partial_{x^j} g_{ik} - \partial_{x^k} g_{ij}\right)/2$ (the Levi–Civita connection). Taking the derivative of the r.h.s. of Eq. (17) along x^k and using Eq. (18) gives the rule of coordinate change for the two Christoffel symbols of the first kind Γ_{kij} and Γ_{kji}, written for Γ_{kij} as

$$\Gamma_{kij} = \partial^2_{x^k x^i} \widetilde{x}^\alpha \, \partial_{x^j} \widetilde{x}^\beta \, \widetilde{g}_{\alpha\beta} + \partial_{x^k} \widetilde{x}^\nu \, \partial_{x^i} \widetilde{x}^\alpha \, \partial_{x^j} \widetilde{x}^\beta \, \widetilde{\Gamma}_{\nu\alpha\beta} \,, \tag{19}$$

where $\widetilde{\Gamma}_{\nu\alpha\beta}$ denote the Christoffel symbols of the first kind associated with the metric $\widetilde{g}_{\alpha\beta}$. It follows that this rule of change of coordinate (19) summarises by itself the constraint corresponding to the change of metric under the action of the change of coordinate. The second-order derivatives are then given by

$$\partial^2_{x^k x^i} \widetilde{x}^\mu = \widetilde{g}^{\gamma\mu} \, \partial_{\widetilde{x}^\gamma} x^j \, \Gamma_{kij} - \partial_{x^k} \widetilde{x}^\nu \, \partial_{x^i} \widetilde{x}^\alpha \, \widetilde{\Gamma}^\mu_{\nu\alpha} \,, \tag{20}$$

where $\widetilde{\Gamma}^\mu_{\nu\alpha} = \widetilde{\Gamma}_{\nu\alpha\gamma} \, \widetilde{g}^{\gamma\mu}$ are the Christoffel symbols of the second kind, with $\widetilde{g}^{\gamma\mu}$ the inverse matrix of $\widetilde{g}_{ij}$, i.e. $\widetilde{g}^{\alpha\beta} \, \widetilde{g}_{\beta\gamma} = \delta_{\alpha\gamma}$.

In Eq. (20), the derivative $\partial_{\widetilde{x}^\gamma} x^j$ can be computed from the inverse of the tensor $\partial_{x^i} \widetilde{x}^\beta$. However, another direct expression can be obtained using Eq. (17), from which it is easy to determine that $\widetilde{g}^{\gamma\mu} \, \partial_{\widetilde{x}^\gamma} x^j = \partial_{x^l} \widetilde{x}^\mu \, g^{lj}$, which leads to

$$\partial^2_{x^k x^i} \widetilde{x}^\mu = \Gamma^l_{ki} \, \partial_{x^l} \widetilde{x}^\mu - \partial_{x^k} \widetilde{x}^\nu \, \partial_{x^i} \widetilde{x}^\alpha \, \widetilde{\Gamma}^\mu_{\nu\alpha} \,, \tag{21}$$

with $\Gamma^l_{ki} = g^{lj} \Gamma_{kij}$ the Christoffel symbol of the second kind associated with the metric g_{ij}. From these second-order derivatives, we obtain a coupled system of Poisson-like equations

$$\Delta \widetilde{x}^\mu = \Gamma^l_{kk} \, \partial_{x^l} \widetilde{x}^\mu - \partial_{x^k} \widetilde{x}^\nu \, \partial_{x^k} \widetilde{x}^\alpha \, \widetilde{\Gamma}^\mu_{\nu\alpha} \,, \tag{22}$$

where Γ^l_{kk} ($\widetilde{\Gamma}^\mu_{\nu\alpha}$) is evaluated at $\mathbf{x}$ ($\widetilde{\mathbf{x}}(\mathbf{x})$) and with $\Delta = \sum_k \partial^2_{x^k x^k}$ (i.e. not the Beltrami operator). By symmetry of the change of variable, we obtain a similar coupled system for the components x^μ

$$\Delta x^\mu = \widetilde{\Gamma}^l_{kk} \, \partial_{\widetilde{x}^l} x^\mu - \partial_{\widetilde{x}^k} x^\nu \, \partial_{\widetilde{x}^k} x^\alpha \, \Gamma^\mu_{\nu\alpha} \,, \tag{23}$$

where Γ^l_{kk} ($\widetilde{\Gamma}^\mu_{\nu\alpha}$) is evaluated at $\mathbf{x}(\widetilde{\mathbf{x}})$ ($\widetilde{\mathbf{x}}$).

We now apply Eqs (22) and (23) to find the isotropization deformation.

3.3. Global equation of global isotropization

Knowing the metric field $\mathbf{g}$, the global isotropization issue aims to find an isotropization deformation $\widetilde{\mathbf{x}} = \overset{\circ}{D}(\mathbf{x})$ so that the metric field $\widetilde{\mathbf{g}}$ is constant, and equal to $\widetilde{\mathbf{g}}_{\mathbf{x}} = \widetilde{L}_h^{-2} \mathbf{I}$ for all $\mathbf{x}$, where $\widetilde{L}_\mathrm{h}$ is an unknown length-scale.

Since the metric field $\widetilde{\mathbf{g}}$ is constant, it follows that its Christoffel symbols $\widetilde{\Gamma}^\mu_{\nu\alpha}$ are zero. Hence, the nonlinear coupled system Eq. (22) takes the form of a linear non-coupled system

$$\Delta \widetilde{x}^\mu = \Gamma^l_{kk} \, \partial_{x^l} \widetilde{x}^\mu. \tag{24}$$

This system does not require any information from the metric $\widetilde{\mathbf{g}}$. In particular, the length-scale $\widetilde{L}_\mathrm{h}$ has disappeared, meaning that this length is completely determined by the coordinate transform, and is obtained as a result of Eq. (24).

In one dimension, Eq. (24) becomes

$$\partial^2_x \overset{\circ}{D} = \left(-\frac{1}{L} \partial_x L\right) \partial_x \overset{\circ}{D} \,,$$

where $L(x)$ denotes the diagnosed 1D length-scale, so that $g_{11} = L^{-2}$ and $g^{11} = L^2$, leading to $\Gamma_{111} = -L^{-3} \partial_x L$ and $\Gamma^1_{11} = g^{11} \Gamma_{111} = -L^{-1} \partial_x L$; this is no more than Eq. (15).

In two dimensions, Eq. (24) is

$$\left.\begin{aligned} \Delta \overset{\circ}{D}_1 &= \Gamma^1_{kk} \partial_x \overset{\circ}{D}_1 + \Gamma^2_{kk} \partial_y \overset{\circ}{D}_1, \\ \Delta \overset{\circ}{D}_2 &= \Gamma^1_{kk} \partial_x \overset{\circ}{D}_2 + \Gamma^2_{kk} \partial_y \overset{\circ}{D}_2, \end{aligned}\right\} \tag{25}$$

where $\Gamma^1_{kk} = \Gamma^1_{11} + \Gamma^1_{22}$ and $\Gamma^2_{kk} = \Gamma^2_{11} + \Gamma^2_{22}$, also expressed in terms of displacement fields $\overset{\circ}{D}_i(\mathbf{x}) = x^i + \overset{\circ}{d}_i(\mathbf{x})$

$$\left.\begin{aligned} \Delta \overset{\circ}{d}_1 &= \Gamma^1_{kk}(1 + \partial_x \overset{\circ}{d}_1) + \Gamma^2_{kk} \partial_y \overset{\circ}{d}_1, \\ \Delta \overset{\circ}{d}_2 &= \Gamma^1_{kk} \partial_x \overset{\circ}{d}_2 + \Gamma^2_{kk}(1 + \partial_y \overset{\circ}{d}_2). \end{aligned}\right\} \tag{26}$$

The system is equivalent to the one found by Michel (2013a) (Eqs (29)–(30)) but, in this case, scalar coefficients Γ^i_{kk} are deduced from the estimation of the local metric $\mathbf{g}$ (the length-scale) in place of the wavelet estimation.

For a connected and simply connected domain (any loop can be continuously contracted to a point), a necessary and sufficient condition for the existence of a solution to Eq. (24) is that the Riemann curvature tensor

$$R^m_{kij} = \partial_{x^i} \Gamma^m_{jk} - \partial_{x^j} \Gamma^m_{ik} + \Gamma^n_{jk} \Gamma^m_{in} - \Gamma^n_{jk} \Gamma^m_{in}$$

is everywhere zero (Ciarlet, 2006). It means that the Gauss curvature of the Riemann manifold defined by the field of metric $\mathbf{g}$ is zero, and that the Riemann manifold is a flat manifold (like $\mathbb{R}^n$).

Of course, this appears as a serious limitation for applications in data assimilation where the Riemann curvature may not necessarily be zero. For instance, the metric field associated with locally isotropic correlations takes the form $\mathbf{g}_\mathbf{x} = L(\mathbf{x})^{-2} \mathbf{I}$, where $L(\mathbf{x})$ is a function of space, and defines a curved manifold for which the Gauss curvature, in 2D, is $K(\mathbf{x}) = L(\mathbf{x})^2 \Delta \log L(\mathbf{x})$, which is *a priori* not zero; no coordinate transformation will be able to lead to a global isotropic correlation. This leads us to relax the aim of a global isotropization towards a local one.

3.4. Global equation of local isotropization in 2D

While global isotropization aims to find a metric field such that $\widetilde{\mathbf{g}}_\mathbf{x} = \widetilde{L}_\mathrm{h}^{-2} \mathbf{I}$ with $\widetilde{L}_\mathrm{h}$ constant, local isotropization only imposes $\widetilde{\mathbf{g}}_\mathbf{x} = \widetilde{L}(\widetilde{\mathbf{x}})^{-2} \mathbf{I}$ with $\widetilde{L}(\widetilde{\mathbf{x}})$ a function of space.

The use of Eq. (22) to find a local isotropization coordinate transform seems of little interest; in general the metric $\widetilde{\mathbf{g}}_{\widetilde{\mathbf{x}}}$ leads to a curved manifold. This implies that the Christoffel symbols $\widetilde{\Gamma}^\mu_{\nu\alpha}$ are not zero, but these coefficients are not directly available from data.

For the 2D case, the Christoffel symbols of the second kind of a locally isotropic metric field $\widetilde{\mathbf{g}}_\mathbf{x} = \widetilde{L}(\widetilde{\mathbf{x}})^{-2} \mathbf{I}$ satisfy $\widetilde{\Gamma}^1_{kk} = 0$ and $\widetilde{\Gamma}^2_{kk} = 0$. This suggests using Eq. (23) in place of Eq. (22) to find the coordinate transform.

This leads to a two-step algorithm, starting (step 1) by resolving Eq. (23) in 2D

$$\Delta \overset{\circ}{D}{}^{-1}_i = -\Gamma^i_{\nu\alpha} \partial_{\widetilde{x}^k} \overset{\circ}{D}{}^{-1}_\nu \, \partial_{\widetilde{x}^k} \overset{\circ}{D}{}^{-1}_\alpha \,, \tag{27}$$

leading to $\mathbf{x}(\widetilde{\mathbf{x}}) = \left(\overset{\circ}{D}_1^{-1}(\widetilde{\mathbf{x}}), \overset{\circ}{D}_2^{-1}(\widetilde{\mathbf{x}})\right)$ (for periodic boundary conditions, this equation is solved in terms of displacement fields), then (step 2) by inverting the resulting coordinate transform to obtain $\widetilde{\mathbf{x}}(\mathbf{x}) = \left(\overset{\circ}{D}_1(\mathbf{x}), \overset{\circ}{D}_2(\mathbf{x})\right)$ and deduce the locally isotropic metric field $\widetilde{\mathbf{g}}$.

3.5. *Case of small deformations*

The Jacobian of the deformation $\overset{\circ}{D}(\mathbf{x}) = \mathbf{x} + \overset{\circ}{d}(\mathbf{x})$ is given by

$$\overset{\circ}{\mathbf{D}}_{\mathbf{x}} = \mathbf{I} + \overset{\circ}{\mathbf{F}}_{\mathbf{x}},$$

where $\overset{\circ}{\mathbf{F}}_{\mathbf{x}}$ denotes the Jacobian of displacements $\overset{\circ}{d}$ at position $\mathbf{x}$. The assumption of small deformations corresponds to the case where $\gamma \ll 1$ with $\gamma = \max_{\mathbf{x}}|||\mathbf{F}_{\mathbf{x}}|||$, and $|||\cdot|||$ is the subordinate matrix norm associated with $||\cdot||$ defined as $|||\mathbf{F}||| = \max_{||\mathbf{e}||=1}||\mathbf{Fe}||$.

Under the assumption of small deformations, the first-order derivatives of the displacement field are switched off. In 2D, Eq. (26) then becomes

$$\left.\begin{aligned} \Delta\,\overset{\circ}{d}_1 &= \Gamma^1_{kk}, \\ \Delta\,\overset{\circ}{d}_2 &= \Gamma^2_{kk}. \end{aligned}\right\} \tag{28}$$

This corresponds to the zero-order approximation which holds without distinction for the global and the local isotropization procedure.

3.6. *Numerical recipes for solving the isotropization problem*

From the previous paragraph, the deformation equation (coordinate transform) requires solving Eq. (25) or Eq. (27) which can be considered as a particular form of Eq. (22). A practical trick for solving Eq. (22) is to introduce a pseudo-diffusion scheme (Eells and Sampson, 1964; Smolarkiewicz and Margolin, 1994), where the components $\widetilde{x}^\nu$ in Eq. (25) (x^ν in Eq. (27)) are steady-state solutions in pseudo-time τ of the diffusion equation

$$\partial_\tau \widetilde{x}^\mu = \Delta\widetilde{x}^\mu - \Gamma^l_{kk}\,\partial_{x^l}\widetilde{x}^\mu + \partial_{x^k}\widetilde{x}^\nu\,\partial_{x^k}\widetilde{x}^\alpha\,\widetilde{\Gamma}^\mu_{\nu\alpha}. \tag{29}$$

The numerical solution of Eq. (29) can be obtained from the time discretization using an Euler scheme

$$\widetilde{\mathbf{x}}_{q+1} = \widetilde{\mathbf{x}}_q + \mathrm{d}\tau\,\mathcal{M}(\widetilde{\mathbf{x}}_q), \tag{30}$$

where $\mathcal{M}(\widetilde{\mathbf{x}}_q)$ denotes the discretization of the r.h.s. term of Eq. (29) and $\widetilde{\mathbf{x}}_q$ is the discretized version of the components $(\widetilde{\mathbf{x}}^\mu)$ at time $\tau = q\mathrm{d}\tau$. This approach can be viewed as a fixed-point method applied to

$$\widetilde{\mathbf{x}} = \mathcal{F}(\widetilde{\mathbf{x}}) = \widetilde{\mathbf{x}} + \mathrm{d}\tau\,\mathcal{M}(\widetilde{\mathbf{x}}). \tag{31}$$

For the numerical experiments, the discretization of first-order derivatives is performed with a second-order scheme, e.g. for a field α the derivative along the x-direction at point (x_i, y_j) is given by:

$$(\partial_x\alpha)_{ij} = \frac{1}{2\delta l}\big[\alpha(x_i+\delta l, y_j) - \alpha(x_i-\delta l, y_j)\big],$$

where δl is the space resolution of the regular coordinate system, while the Laplacian is discretized as

$$(\Delta\alpha)_{ij} = \frac{1}{\delta l^2}\big[\alpha(x_i+\delta l, y_j) + \alpha(x_i-\delta l, y_j) + \alpha(x_i, y_j+\delta l) + \alpha(x_i, y_j-\delta l) - 4\alpha(x_i, y_j)\big].$$

Furthermore, for the space discretization δl, the time step of the diffusion $\partial_\tau\alpha = \nu\Delta\alpha$ can be deduced from $\delta\alpha/\delta\tau = \nu\delta\alpha/\delta l^2$ as $\delta\tau = \delta l^2/\nu$. It follows that the numerical value of $\mathrm{d}\tau$, with $\nu = 1$ is $\mathrm{d}\tau = \delta l^2/4$, where the factor $1/4$ is introduced due to the CFL condition (Weaver and Courtier, 2001). The integration in time is achieved over 1000 time steps $\mathrm{d}\tau$, corresponding to a long time integration as required to find the steady-state solution.

The isotropization procedure is illustrated within a 2D setting in the next section.

4. Numerical experiments

4.1. *Experimental set-up*

Anisotropic correlations are now numerically constructed in 2D from globally isotropic ones with a deformation derived from an arbitrary stream function. This construction will be used to test the skill of both global and local isotropization methods.

In this 2D experiment, we consider the bi-periodic domain $[0, 1000\,\mathrm{km}] \times [0, 1000\,\mathrm{km}]$ discretized in $n = 81$ points along the two directions x and y, so that $\mathrm{d}x = \mathrm{d}y \approx 12\,\mathrm{km}$. A deformation $D(\mathbf{x}) = \mathbf{x} + d(\mathbf{x})$ is constructed with the displacement field $\mathrm{d}(x) = \mathbf{u}(\mathbf{x})\mathrm{d}t$ deduced from a wind $\mathbf{u}_0(\mathbf{x}) = \mathbf{k} \times \nabla\psi$, where ψ is a stream function, and normalized so that

$$\mathbf{u} = (u, v) = \left\{\frac{u_0}{\max(|u_0|)}, \frac{v_0}{\max(|v_0|)}\right\}.$$

With this definition, $\max\{d_1(\mathbf{x})\} = \max\{d_2(x)\} = \mathrm{d}t$, hence the magnitude of the wind-like deformation is controlled by $\mathrm{d}t$. The strength of the deformation is quantified by

$$\gamma(\mathrm{d}t) = \max_{\mathbf{x}}|||\mathbf{F}_{\mathbf{x}}|||, \tag{32}$$

where $\mathbf{F}_{\mathbf{x}}$ is the Jacobian matrix of d at $\mathbf{x}$ for $\mathrm{d}t$, and $|||\mathbf{F}||| = \max_{||\mathbf{e}||=1}||\mathbf{Fe}||$ is the subordinate matrix norm induced by the norm $||\cdot||$. Note that $\gamma(\mathrm{d}t) = \mathrm{d}t \times \gamma(1)$.

For numerical experiments, the stream function used is shown in Figure 1, and the magnitude of $\mathrm{d}t$ is either $\mathrm{d}t = 0.03 = 2.4\mathrm{d}x$ or $\mathrm{d}t = 0.05 = 4\mathrm{d}x$. Numerical computation of $\gamma(1) \approx 22.4$ implies that $\gamma(\mathrm{d}t = 0.03) \approx 0.67$ while $\gamma(\mathrm{d}t = 0.05) \approx 1.12$. The assumption of small deformations requires that $\gamma(\mathrm{d}t) \ll 1$ (section 3.5), thus the deformation for $\mathrm{d}t = 0.03$ ($\mathrm{d}t = 0.05$) is considered as small (large). Figure 2(a) illustrates the wind-like deformation of the regular coordinate system for $\mathrm{d}t = 0.05$.

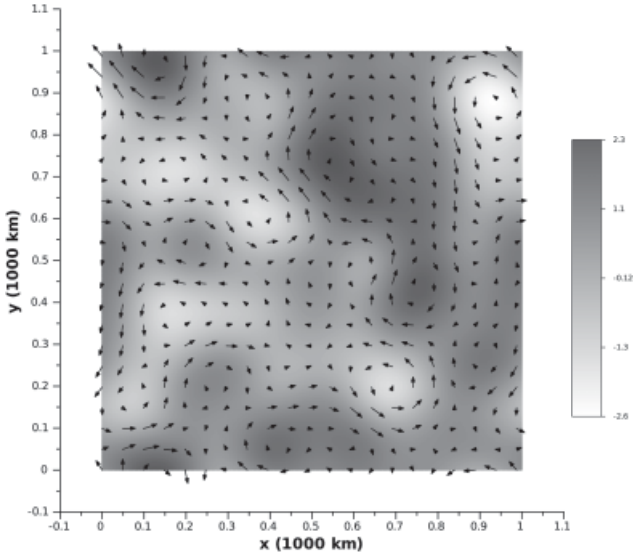

Figure 1. Stream function used to create the displacement field. The arrows indicate the direction and the intensity of the associated displacement.

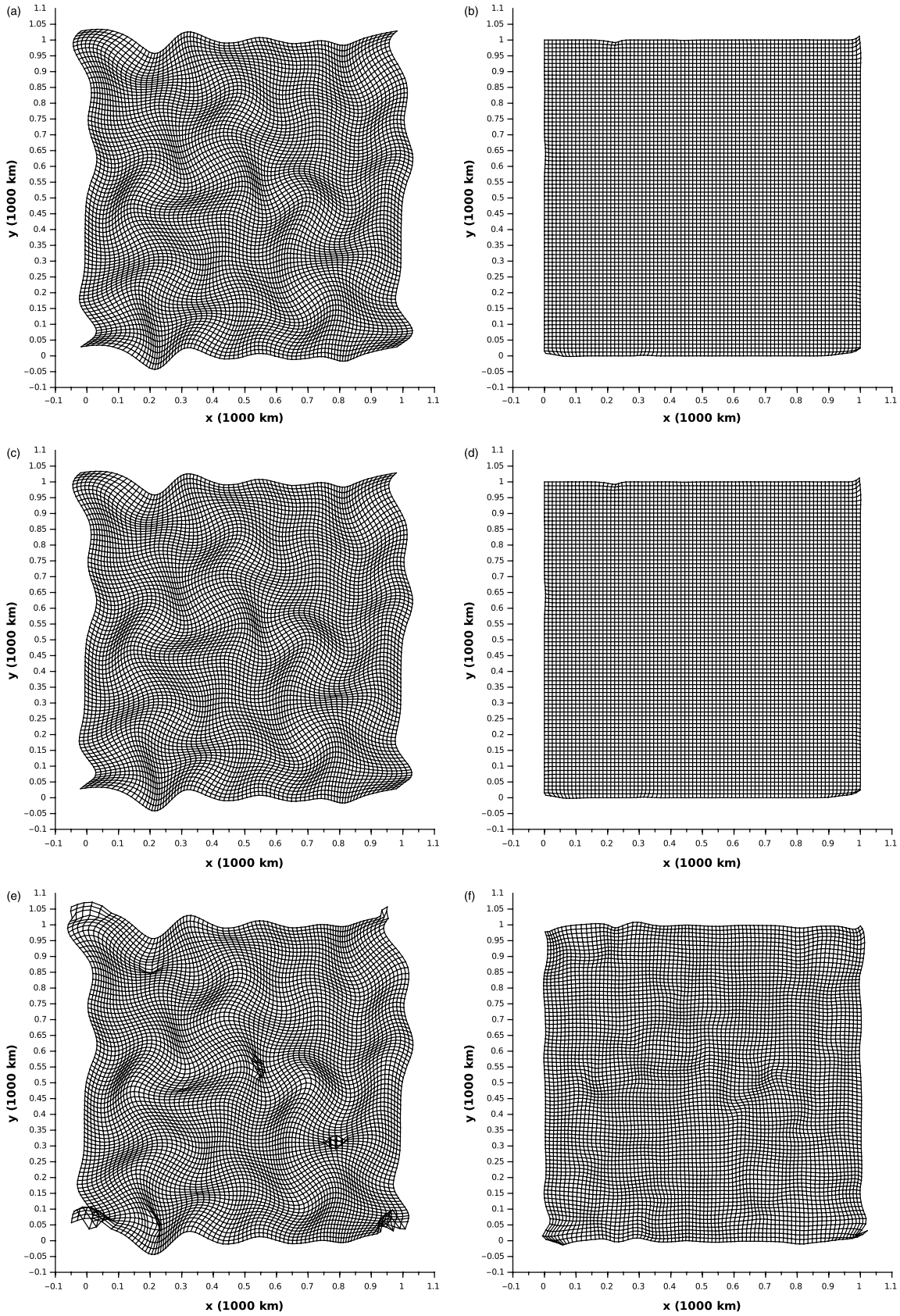

Figure 2. For d$t = 0.05$, deformation of the regular coordinate system by the action of the deformation (a) D, (c) $\overset{\circ}{D}^{-1}$ and (e) $\overset{\circ}{D}_s^{-1}$. Deformation of the deformed coordinate system (a) by the action of the deformation (b) D^{-1}, (d) $\overset{\circ}{D}$ and (f) $\overset{\circ}{D}_s$. See text for details.

Heterogeneous correlations ρ_D are deduced from isotropic ones, defined by

$$\rho_{\mathrm{h}}(\mathbf{x},\mathbf{y}) = \exp\left(\frac{-||\mathbf{x}-\mathbf{y}||^2}{2L_{\mathrm{h}}^2}\right),$$

where $L_{\mathrm{h}} = 50\,\mathrm{km} \approx 4\mathrm{d}x$, by the action of the wind-like deformation D on ρ_{h} according to Eq. (4).

4.2. *Validation of the local length-scale dynamics*

As a first validation, we show that Eq. (10) provides an accurate approximation for the length-scales of the deformed correlations. A randomization strategy (Fisher and Courtier, 1995) has been employed in order to compute the reference.

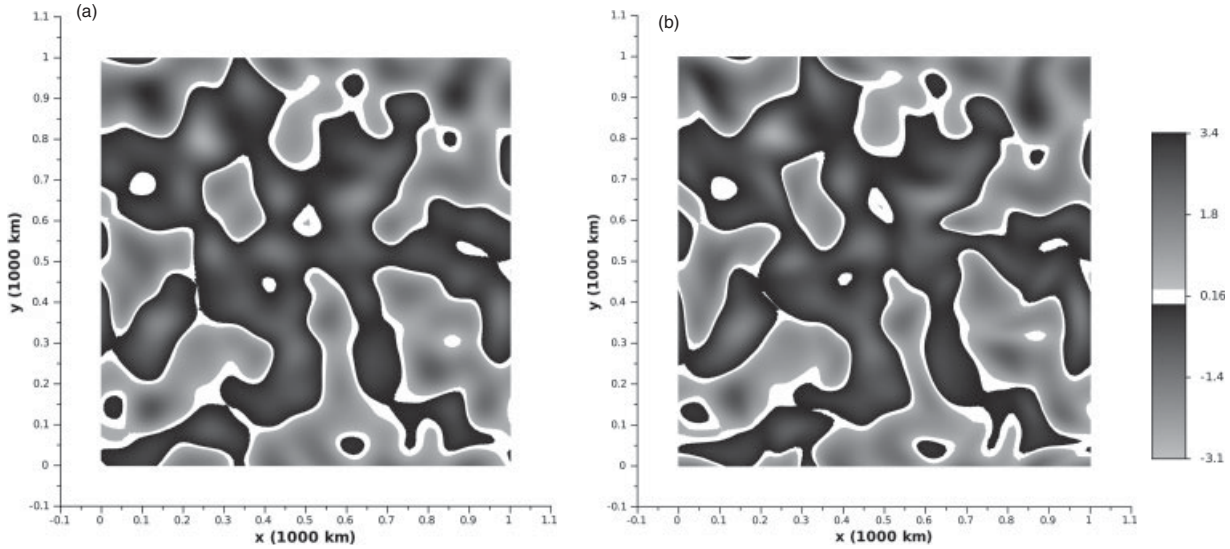

Figure 3. Example of one realization of (a) an homogeneous-isotropic error of length-scale $L_{\rm h} = 50$km, and (b) its deformed version for $\mathrm{d}t = 0.05$.

For that purpose, a large ensemble $(\widetilde{\boldsymbol{\epsilon}^{\rm b}}_k)_{k\in[1,Ne]}$, of auto-correlation $\widetilde{\rho}$, has been constructed from an ensemble of homogeneous errors $(\boldsymbol{\epsilon}^{\rm b}{}_k)_{k\in[1,Ne]}$, of auto-correlation ρ_h, as $\widetilde{\boldsymbol{\epsilon}^{\rm b}}_k(\widetilde{\mathbf{x}}) = \boldsymbol{\epsilon}^{\rm b}\left[D^{-1}(\widetilde{\mathbf{x}})\right]$. Figure 3 represents (a) a homogeneous sample error $\boldsymbol{\epsilon}^{\rm b}$ and (b) its deformed version $\widetilde{\boldsymbol{\epsilon}^{\rm b}}$ (with $\mathrm{d}t = 0.05$), where the transport by the wind-like advection is visible. The length-scales estimated from this ensemble are taken as a reference for comparison.

In the numerical experiments, $Ne = 6400$, leading to a sampling error of order $\mathcal{O}(1/\sqrt{Ne})$ with $1/\sqrt{Ne} \approx 0.012$. The resulting estimation can be considered as being quite similar to the theoretical exact value. Hence, the numerical estimation is taken as a reference. In real applications, such a huge ensemble size is not affordable and filtering strategies are employed to damp down the sampling noise (Berre *et al.*, 2007; Raynaud *et al.*, 2009). Raynaud and Pannekoucke (2013) detail the length-scale sampling noise properties and its filtering.

Similarly to Pannekoucke (2009), the ensemble estimation of the local metric tensors $\widetilde{\mathbf{g}}_{\widetilde{\mathbf{x}}}$ is deduced from the grid-point estimation of local correlations $\widetilde{\rho}(\widetilde{\mathbf{x}}, \widetilde{\mathbf{x}} + \delta\widetilde{\mathbf{x}})$ where $\delta\widetilde{\mathbf{x}} = (\mathrm{d}\widetilde{x}, \mathrm{d}\widetilde{y})$ for $\mathrm{d}\widetilde{x} \in \{-\mathrm{d}x, 0, \mathrm{d}x\}$ and $\mathrm{d}\widetilde{y} \in \{-\mathrm{d}y, 0, \mathrm{d}y\}$: $\widetilde{\mathbf{g}}_{\widetilde{\mathbf{x}}}$ is the least-square solution of the system $||\delta\widetilde{\mathbf{x}}||_{\widetilde{\mathbf{g}}_{\widetilde{\mathbf{x}}}} \approx f\,[\widetilde{\rho}(\widetilde{\mathbf{x}}, \widetilde{\mathbf{x}} + \delta\widetilde{\mathbf{x}})]$, with $f(r) = 2(1 - r)$ under the parabola-based approximation (Pannekoucke *et al.*, 2008). The length-scale fields along directions x and y are deduced from the local metric tensor $\mathbf{g}_{\widetilde{\mathbf{x}}}$ by

$$L_x(\widetilde{\mathbf{x}}) = \frac{1}{\sqrt{\widetilde{g}_{11}}} \text{ and } L_y(\widetilde{\mathbf{x}}) = \frac{1}{\sqrt{\widetilde{g}_{22}}},$$

where $\widetilde{g}_{ij}(\widetilde{\mathbf{x}}) = (\widetilde{\mathbf{g}}_{\widetilde{\mathbf{x}}})_{ij}$.

The illustration of the ability of the analytical formula to represent the transport is now examined from the anisotropy diagnosis. Figure 4 represents local ellipses associated with the local tensor $\widetilde{\mathbf{g}}_{\widetilde{\mathbf{x}}}^{-1}$ deduced (a) from the analytical formula Eq. (10), and (b) from the ensemble estimation. The larger the eccentricity of the ellipse, the stronger the anisotropy. A null eccentricity is equivalent to an isotropic correlation and leads to a circle. Moreover, the major axis of the ellipse defines the direction of the largest elongation of the correlation function. There is no significant difference between these two fields, showing that the analytical formula provides an accurate representation of the transport in this experiment.

The analytical formula is thus able to reproduce accurate deformed length-scales, as regards anisotropic features of the correlation functions.

4.3. *Isotropization procedure*

4.3.1. *Test of the global isotropization procedure*

This section examines the ability of the previously proposed algorithm to find a global isotropizing deformation. It consists of computing the isotropizing deformation knowing the local metric tensor $\mathbf{g}_{\mathbf{x}}$, illustrated in Figure 4(a) and to confirm that, in the resulting change of coordinate, the metric is transformed into an isotropic one $\widetilde{\mathbf{g}}_{\widetilde{\mathbf{x}}} = L_{\rm h}^{-2}\mathbf{I}$.

Here, ρ_D denotes the correlation functions deduced from the wind-like deformation of the isotropic correlation functions $\rho_{\rm h}$ by the deformation D; $\rho_{\overset{\circ}{D}}$ denotes the correlation functions deduced from the global isotropization of ρ_D as obtained with the two strategies detailed in sections 3.3 and 3.4; $\rho_{\overset{\circ}{D}_s}$ denotes the correlation functions deduced from the global isotropization of ρ_D but under the small deformation assumption, as detailed in section 3.5.

Due to the bi-periodicity, the numerical solution $\overset{\circ}{D}_s$ deduced from Eq. (28) is obtained from a spectral inversion of the Poisson PDE.

For finite deformation, the two algorithms detailed in sections 3.3 and 3.4 can be applied. These two possibilities have been computed and, since the results are similar, we show only those obtained from the solution of Eq. (25). In that case, the computation is made following the pseudo-diffusion strategy detailed in section 3.6, adapted to Eq. (26), leading directly to the isotropozation deformation $\overset{\circ}{D}(\mathbf{x}) = \mathbf{x} + \overset{\circ}{d}(\mathbf{x})$.

Theoretically, since the local metric tensors $\mathbf{g}_{\mathbf{x}}$ have been obtained from the deformation D of constant correlation function $\rho_{\rm h}$, the isotropizing deformation $\overset{\circ}{D}$ should be equal to the inverse deformation D^{-1}, i.e. $\overset{\circ}{D} = D^{-1}$. Conversely, the inverse isotropizing deformation $\overset{\circ}{D}^{-1}$ is the direct deformation D, i.e. $\overset{\circ}{D}^{-1} = D$.

First, the misfit between the numerical deformation and the theoretical one can be quantified from the misfit between the displacement field components $\overset{\circ}{d}_i = \overset{\circ}{D} - id_i$ versus $d_i = D_i - id_i$ for $i = 1, 2$ and where $id(\mathbf{x}) = \mathbf{x}$ denotes the identity function: $||\overset{\circ}{D}_1 - D_1^{-1}||_H = 0.08$ and $||\overset{\circ}{D}_2 - D_2^{-1}||_H = 0.01$ or, in terms of relative error

$$\frac{||\overset{\circ}{D}_1 - D_1^{-1}||_H}{||D_1^{-1} - id_1||_H} = 5\% \text{ and } \frac{||\overset{\circ}{D}_2 - D_2^{-1}||_H}{||D_2^{-1} - id_2||_H} = 1\%,$$

where $||\mathbf{E}||_H = \sqrt{\mathrm{Trace}\,\mathbf{E}^{\rm T}\mathbf{E}}$ denotes the Hilbert norm of matrix $\mathbf{E}$. These scores are much better than those of the

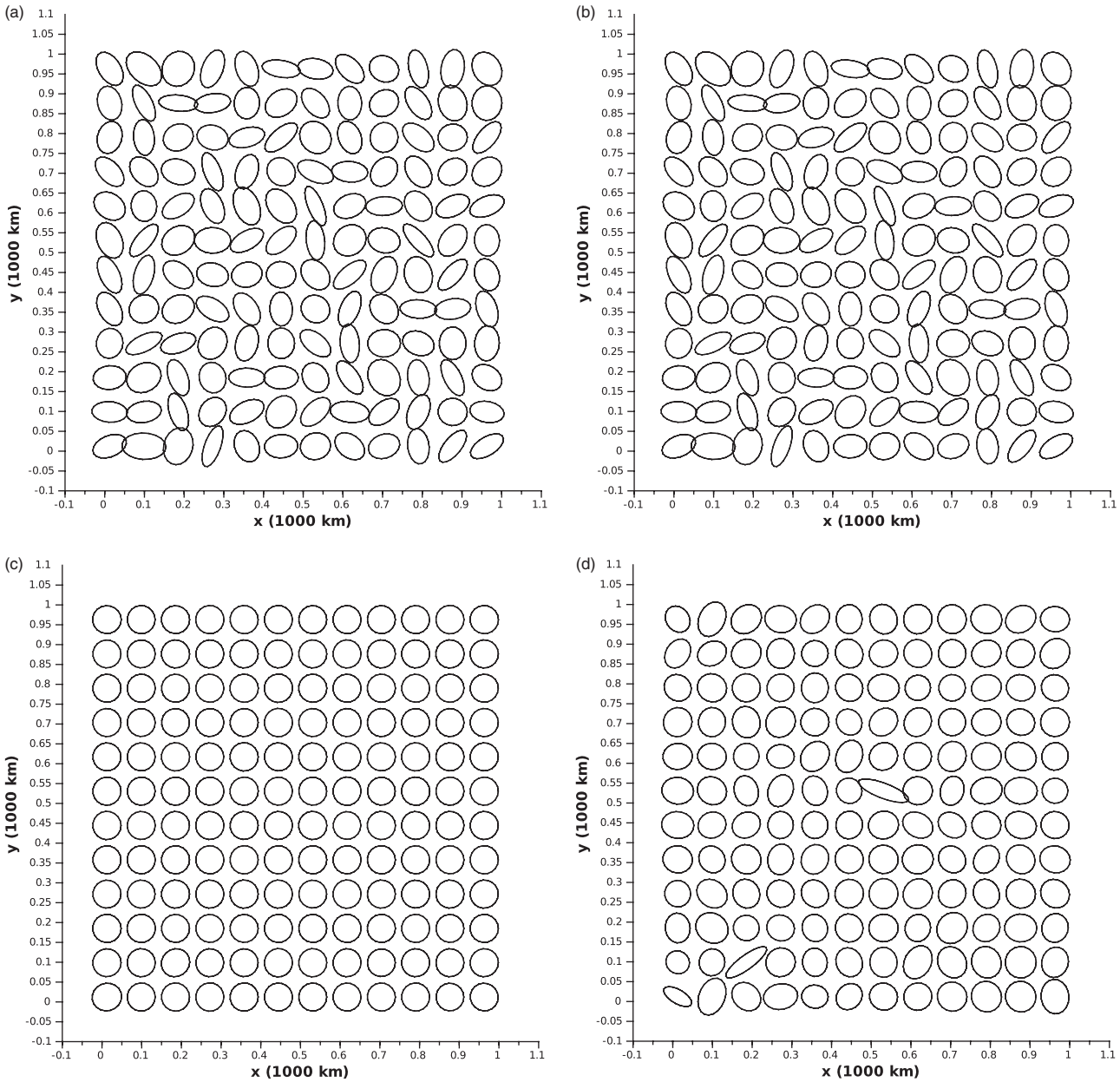

Figure 4. Anisotropy diagnosis for (a) the analytical metric tensor deduced from Eq. (10) and (b) the ensemble diagnosed tensor, for $\mathrm{d}t = 0.05$. (c) shows the local tensor associated with $\rho_{\overset{\circ}{D}}$ and (d) that associated with $\rho_{\overset{\circ}{D}_s}$.

isotropizing deformation $\overset{\circ}{D}_s$, for which $||\overset{\circ}{D}_{s1} - D_1^{-1}||_H = 0.501$ and $||\overset{\circ}{D}_{s2} - D_2^{-1}||_H = 0.504$, or in terms of relative error

$$\frac{||\overset{\circ}{D}_{s1} - D_1^{-1}||_H}{||D_1^{-1} - id_1||_H} = 34.9\% \text{ and } \frac{||\overset{\circ}{D}_{s2} - D_2^{-1}||_H}{||D_2^{-1} - id_2||_H} = 31.9\%.$$

This demonstrates the accuracy of the isotropizing deformation, when computed from the general solution Eq. (27).

The action of the isotropizing deformation $\overset{\circ}{D}$ on the deformed coordinate system by D is represented in Figure 2(d). The resulting coordinate system is relatively similar to that obtained using the theoretical inverse deformation D^{-1} (Figure 2(b)). Moreover, the action of the inverse isotropizing deformation $\overset{\circ}{D}^{-1}$ on the regular coordinate system (Figure 2(c)) is equivalent to the action of the theoretical deformation D (Figure 2(a)). The results obtained with the deformation $\overset{\circ}{D}_s$ are represented in Figure 2(f) and (e). We observe that the action of $\overset{\circ}{D}_s$ produces a less regular coordinate system than $\overset{\circ}{D}$ (compare Figure 2(f) and (d)). Differences in the deformed coordinate system are also visible (compare Figure 2(e) and (c)).

In terms of length-scale, the isotropizing deformation $\overset{\circ}{D}$ applied to ρ_D should lead to homogeneous correlations of length-scale L_h. Figure 5 presents the diagnosed length-scales of $\rho_{\overset{\circ}{D}}$ along x (Figure 5(c)) and y (Figure 5(d)). On average, the resulting length-scales are relatively homogeneous, with values mostly within 5% of L_h. The length-scales associated with the correlation $\rho_{\overset{\circ}{D}_s}$ are represented in Figure 5(e, f). In that case, the length-scales are far from being homogeneous, as shown by the large deviations from the expected value $L_\mathrm{h} = 50$ km.

Figure 4 illustrates the effect of the isotropizing deformation in terms of anisotropy. The anisotropic ellipses of the correlations ρ_D (Figure 4(a)) are transformed by $\overset{\circ}{D}$ into quasi-circular ellipses (Figure 4(c)). When using the deformation $\overset{\circ}{D}_s$ (Figure 4(d)), the resulting ellipses are not so far from circles, except in regions where the isotropization under the small deformations assumption has failed.

Note that, for less intense deformation ($\mathrm{d}t = 0.03$), the solution resulting from the small-deformation assumption succeeds in finding the inverse deformation with an acceptable accuracy. This result is shown in the next section for the local isotropization procedure.

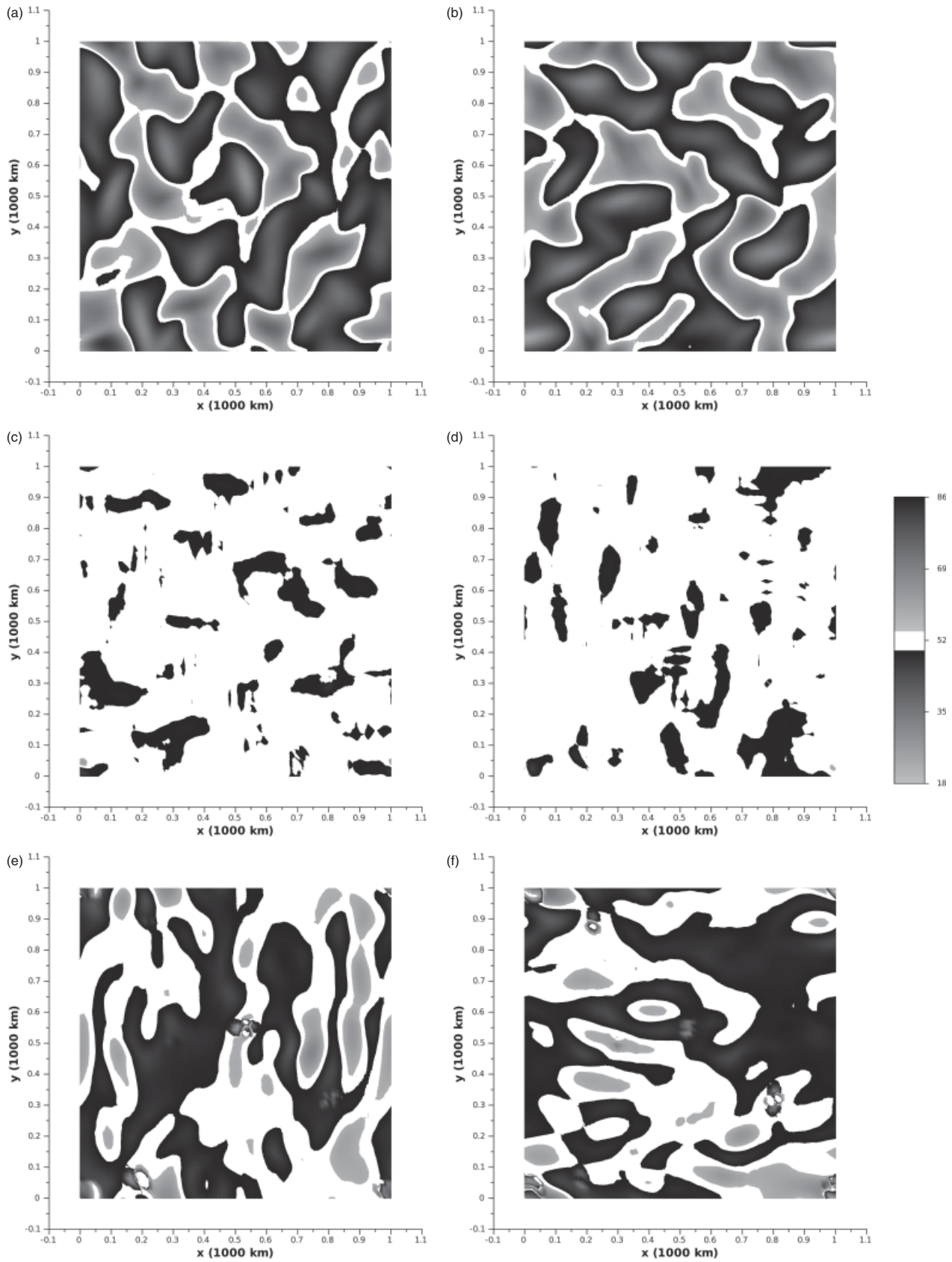

Figure 5. Length-scales (km) (a, c, d) along direction x and (b, e, f) along y. (a, b) show length-scales diagnosed from the analytical formulation Eq. (10); (c, d) length-scales obtained after the isotropization procedure (solution of Eq. (25)); and (e, f) length-scales obtained under the assumption of small deformations (Eq. (28)).

4.3.2. *Test of the local isotropization procedure*

This subsection focuses on the local isotropizing deformation in the case where the initial isotropic correlation ρ_{h} is replaced by locally isotropic correlation functions described by the metric field $\mathbf{g}_{\mathbf{x}} = L(\mathbf{x})^{-2}\mathbf{I}$, where $L(\mathbf{x}) = L_h\left[1 + 0.5\sin(kx)\sin(ky)\right]$ with $k = 2\pi/1000$ km.

The notation introduced in the previous paragraph is kept except for ρ_D which denotes now the correlation functions obtained from the deformation of correlation functions of metric $\mathbf{g}_{\mathbf{x}} = L(\mathbf{x})^{-2}\mathbf{I}$.

The numerical solution of the isotropizing deformation $\overset{\circ}{D}$ is computed from the two-step algorithm detailed in section 3.4, which computes the inverse deformation $\overset{\circ}{D}^{-1}$ from the numerical

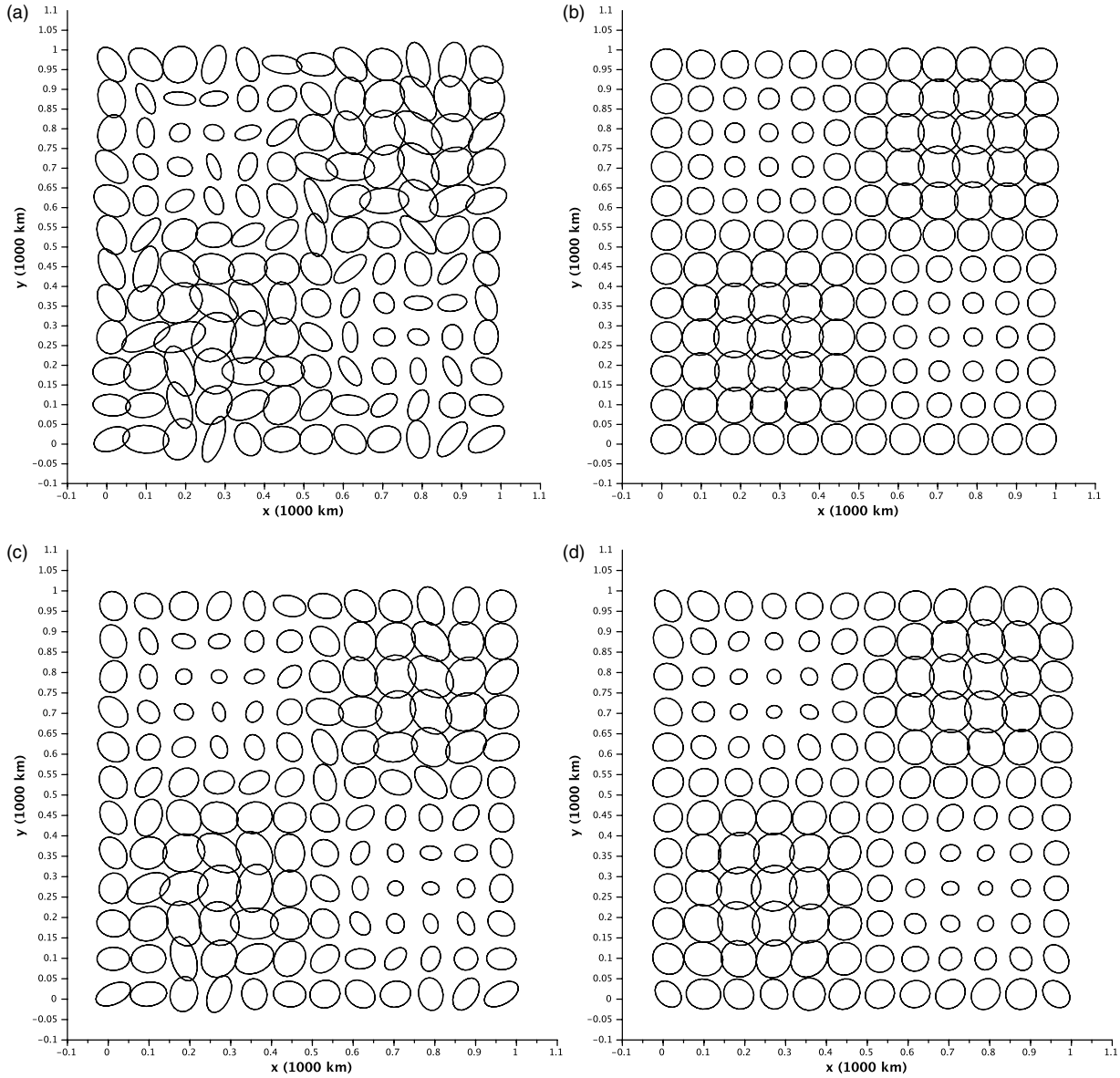

Figure 6. Illustration of the local isotropization in terms of anisotropy diagnosis. For $\mathrm{d}t = 0.05$: (a) initial local anisotropic tensor associated with ρ_D, and (b) local isotropic tensor associated with $\rho_{\overset{\circ}{D}}$. For $\mathrm{d}t = 0.03$: (c) initial local anisotropic tensor associated with ρ_D, and (d) local quasi-isotropic tensor associated with $\rho_{\overset{\circ}{D}_s}$ under the small-deformation assumption.

solution of Eq. (27), rather than the direct deformation $\overset{\circ}{D}$ from the fixed-point method detailed in section 3.1.

Figure 6 illustrates the results in terms of anisotropy diagnosis for two situations: the finite-deformation case where $\mathrm{d}t = 0.05$ and then the small-deformation case where $\mathrm{d}t = 0.03$. From the initial anisotropic metric, Figure 6(a), the two-step algorithm (section 3.4) leads to a coordinate change which transforms the anisotropic metric into a locally isotropic one (Figure 6(b)), where the theoretical metric $\mathbf{g}_{\mathbf{x}} = L(\mathbf{x})^{-2}\mathbf{I}$ is obtained with a good accuracy.

To illustrate the ability of the small-deformation algorithm to recover the local isotropic metric, we also consider the small-deformation case where $\mathrm{d}t = 0.03$. This time, from the initial metric (Figure 6(c)), the numerical solution $\overset{\circ}{D}_s$ of Eq. (28) leads to a quasi-locally isotropic metric (Figure 6(d)). The local metric is not perfectly circular since some ellipses are still present, but remains in accordance with the theoretical metric $\mathbf{g}_{\mathbf{x}} = L(\mathbf{x})^{-2}\mathbf{I}$.

From these illustrations, the two-step algorithm (section 3.4) is shown able to accurately estimate the isotropizing deformation. Moreover, the small-deformation solution of Eq. (28) has been shown to provide a first insight about the structure of variations of the length-scale field $L(\mathbf{x})$.

5. Applications in data assimilation

Two applications in data assimilation of the above formalism can be mentioned: (i) the modelling of the background-error covariance dynamics through the modelling of length-scale dynamics; and (ii) the background-error covariance modelling using the isotropization process.

5.1. Emulation of the background-error covariance matrix time evolution

It is well known that the costly part of the Kalman filter equations is the time propagation of the analysis covariance matrix $\mathbf{B}_0$ leading to the forecast error covariance matrix $\mathbf{B}_t = \mathbf{M}_t\mathbf{B}_0\mathbf{M}_t^{\mathrm{T}}$ where $\mathbf{M}$ denotes the linear propagator from time 0 to time t, and $\mathbf{M}^{\mathrm{T}}$ its adjoint. The length-scale dynamics resulting by the action of a deformation can be applied to describe the time evolution of the local autocorrelation error shape.

For instance, several chemical species have relatively long lifetimes and can be considered to be passive scalars α, transported by advection/diffusion dynamics

$$\partial_t\alpha + \mathbf{u}\cdot\nabla\alpha = \kappa\,\Delta\alpha\,, \tag{33}$$

where $\mathbf{u}$ is the velocity of the fluid. To facilitate the description of the time evolution of the background-error correlation in chemical data assimilation, one can use the transport formula introduced in section 2.

To understand this, we consider the effect of the advection only:

$$\partial_t \alpha + \mathbf{u} \cdot \nabla \alpha = 0. \tag{34}$$

Due to the linearity of Eq. (34), the same equation governs the time evolution of errors. From a Lagrangian point of view, the time evolution of errors can thus be solved according to the method of characteristics and is equivalent to the deformation of errors by a succession of small deformations $D(\mathbf{x}) = \mathbf{x} + \mathbf{u}(\mathbf{x}, t)\mathrm{d}t$ acting over the time step $\mathrm{d}t$. The evolution of the local metric tensor $\mathbf{g}_{\mathbf{x}}(t)$ which describes the covariance matrix $\mathbf{B}_t$, over a time step $\mathrm{d}t$ is thus given by

$$\mathbf{g}_{\mathbf{x}}(t + \mathrm{d}t) = (\mathbf{D}_{\mathbf{x}}^{-1})^{\mathrm{T}} \mathbf{g}_{D^{-1}(\mathbf{x})}(t) \mathbf{D}_{\mathbf{x}}^{-1}. \tag{35}$$

Note that the variance all along the deformation (or the time integration of Eq. (34)) is conserved in that case.

From this equation, we obtain a flow-dependent characterization of the background-error covariance matrix of passive chemical species without computing explicitly the covariance propagation of the Kalman filter. The numerical cost consists of a nonlinear integration of the model, plus the transport by the wind of the metric field Eq. (35). This cost is quite below the cost of the nonlinear ensemble integration imposed by the ensemble Kalman filter.

5.2. *Background-error covariance modelling*

A second application concerns the use of the isotropization in order to find a coordinate system where statistics are more isotropic (Desroziers, 1997; Michel, 2013a,b) and thus simple to represent with various methods, e.g. the spectral diagonal approach (Courtier *et al.*, 1998), the diffusion operator (Weaver and Courtier, 2001; Pannekoucke and Massart, 2008) or recursive filters (Purser *et al.*, 2003). This is quite attractive from a numerical point of view because isotropy leads to parallelization strategy. For instance in the context of the 2D-homogeneous diffusion operator, the isotropy implies that the pseudo-time integration can be implemented from simple 1D diffusions along the x, then the y directions. For the 1D diffusion along the direction x (y), the lines of constant y (x) are independant and can be integrated in parallel. Moreover, the additional cost associated with the deformation is low since a deformation is implemented as an interpolation.

The present article provides a way to determine a coordinate system in which the statistics are nearly isotropic, using the isotropization procedure which has been introduced in section 3, and supported by the numerical simulations of section 4.

6. Conclusion

In this article, we have described how the length-scale dynamics can be employed to estimate a spatial deformation (coordinate transformation) able to transform anisotropic correlations functions into quasi-isotropic ones.

From the formalism of differential geometry on manifolds, we have deduced necessary conditions for the isotropizing deformation components or the associated displacements. These conditions take the form of Poisson-like PDEs where, in practice, coefficients are deduced from data, e.g. the estimation of the metric tensor from an ensemble and the computation of the associated Christoffel symbol of the second kind.

This Poisson-like system has been solved by introducing a pseudo-diffusion scheme, shown to be similar to a fixed-point method. This solution has then been tested in a simulated 2D setting, using a wind-like deformation that mimics geophysical situations. Anisotropic correlations have been deduced from the action of this wind deformation on globally isotropic correlation functions as well as locally isotropic correlation functions (only the metric tensor has been considered here). The isotropizing deformation has then been computed, based on the diagnosis of the local metric tensor of anisotropic correlations. Theoretically, the isotropizing deformation should be equal to the inverse deformation in that case, offering a way to evaluate the accuracy of the numerical isotropization. The numerical solution is relatively close to the theoretical solution, with a relative error less than 10%. The isotropizing deformation is able to provide isotropic correlations, as shown by the diagnostics of length-scale fields and anisotropy ellipses for instance.

The isotropization procedure has potential applications in geophysical data assimilation for modelling anisotropic correlation functions. Moreover, since it requires only the estimation of the local metric tensor, this approach is an interesting alternative to more complicated wavelet-based methods.

Another application of the length-scale dynamics in data assimilation concerns the time evolution of covariances without explicitly computing the covariance propagation of the Kalman filter. This will be examined in more detail for chemical data assimilation where the dynamics of errors can be linear for particular passive scalars.

Acknowledgements

The authors would like to thank the two anonymous reviewers for their constructive comments. This work was supported by the French LEFE INSU program and the MACC2 project within the FP7 EU research programme.

Appendix A. Derivation of the local metric tensor in the deformed coordinate system

First, the Taylor expansion

$$D^{-1}(\widetilde{\mathbf{x}} + \delta\widetilde{\mathbf{x}}) \underset{\widetilde{\mathbf{x}}}{\approx} D^{-1}(\widetilde{\mathbf{x}}) + \mathbf{D}_{\widetilde{\mathbf{x}}}^{-1} \delta\widetilde{\mathbf{x}} + \mathcal{O}(\delta\widetilde{\mathbf{x}}^2),$$

allows one to write Eq. (3) as

$$\begin{aligned} &||\mathbf{D}_{\widetilde{\mathbf{x}}}^{-1} \delta\widetilde{\mathbf{x}}||^2_{\mathbf{g}_{D^{-1}(\widetilde{\mathbf{x}})}} \\ &= f\left[\rho\{D^{-1}(\widetilde{\mathbf{x}}), D^{-1}(\widetilde{\mathbf{x}}) + \mathbf{D}_{\widetilde{\mathbf{x}}}^{-1} \delta\widetilde{\mathbf{x}}\}\right] + \mathcal{O}(|\delta\widetilde{\mathbf{x}}|^3). \end{aligned}$$

According to the definition of the norm associated with a metric, $||\mathbf{x}||^2_{\mathbf{E}} = \mathbf{x}^{\mathrm{T}}\mathbf{E}\mathbf{x}$, the transformation of $\delta\widetilde{\mathbf{x}}$ by the Jacobian $\mathbf{D}_{\widetilde{\mathbf{x}}}^{-1}$ leads to a change of local metric according to

$$||\mathbf{D}_{\widetilde{\mathbf{x}}}^{-1} \delta\widetilde{\mathbf{x}}||^2_{\mathbf{g}_{D^{-1}(\widetilde{\mathbf{x}})}} = ||\delta\widetilde{\mathbf{x}}||^2_{(\mathbf{D}_{\widetilde{\mathbf{x}}}^{-1})^{\mathrm{T}} \mathbf{g}_{D^{-1}(\widetilde{\mathbf{x}})} \mathbf{D}_{\widetilde{\mathbf{x}}}^{-1}},$$

from which

$$\begin{aligned} &||\delta\widetilde{\mathbf{x}}||^2_{(\mathbf{D}_{\widetilde{\mathbf{x}}}^{-1})^{\mathrm{T}} \mathbf{g}_{D^{-1}(\widetilde{\mathbf{x}})} \mathbf{D}_{\widetilde{\mathbf{x}}}^{-1}} \\ &= f\left[\rho\{D^{-1}(\widetilde{\mathbf{x}}), D^{-1}(\widetilde{\mathbf{x}}) + \mathbf{D}_{\widetilde{\mathbf{x}}}^{-1} \delta\widetilde{\mathbf{x}}\}\right] + \mathcal{O}(|\delta\widetilde{\mathbf{x}}|^3). \end{aligned}$$

By identification with Eq. (9), the local metric tensor $\widetilde{\mathbf{g}}_{\widetilde{\mathbf{x}}}$ is given by

$$\widetilde{\mathbf{g}}_{\widetilde{\mathbf{x}}} = (\mathbf{D}_{\widetilde{\mathbf{x}}}^{-1})^{\mathrm{T}} \mathbf{g}_{D^{-1}(\widetilde{\mathbf{x}})} \mathbf{D}_{\widetilde{\mathbf{x}}}^{-1}. \tag{A.1}$$

Appendix B. Approximation of the Jacobian of the inverse deformation

In practice, the differential operator $\mathbf{D}_{\widetilde{\mathbf{x}}}^{-1}$ can be computed from the Taylor approximation and denoted in matrix form as

$$\mathbf{D}_{\widetilde{\mathbf{x}}}^{-1} \underset{\widetilde{\mathbf{x}}}{\approx} \left[\frac{D^{-1}(\widetilde{\mathbf{x}} + \delta\widetilde{x}\,\mathbf{i}) - D^{-1}(\widetilde{\mathbf{x}})}{\delta\widetilde{x}} \times \frac{D^{-1}(\widetilde{\mathbf{x}} + \delta\widetilde{y}\,\mathbf{j}) - D^{-1}(\widetilde{\mathbf{x}})}{\delta\widetilde{y}}\right], \tag{B.1}$$

where δx (δy) denotes a small positive perturbation along the natural frame direction $\mathbf{i}$ ($\mathbf{j}$). This approximation corresponds to a first-order approximation, while a second-order approximation can be implemented according to

$$\mathbf{D}^{-1}_{\widetilde{\mathbf{x}}} \underset{\widetilde{\mathbf{x}}}{\approx} \left[\frac{D^{-1}(\widetilde{\mathbf{x}} + \delta\widetilde{x}\,\mathbf{i}) - D^{-1}(\widetilde{\mathbf{x}} - \delta\widetilde{x}\,\mathbf{i})}{2\delta\widetilde{x}} \times \frac{D^{-1}(\widetilde{\mathbf{x}} + \delta\widetilde{y}\,\mathbf{j}) - D^{-1}(\widetilde{\mathbf{x}} - \delta\widetilde{y}\,\mathbf{j})}{2\delta\widetilde{y}} \right]. \tag{B.2}$$

This computation can also be achieved from the displacement field d defined by

$$D^{-1}(\widetilde{\mathbf{x}}) = \widetilde{\mathbf{x}} + d^{-1}(\widetilde{\mathbf{x}}), \tag{B.3}$$

so that

$$\mathbf{D}^{-1}_{\widetilde{\mathbf{x}}} \underset{\widetilde{\mathbf{x}}}{\approx} \mathbf{I} + \left[\frac{d^{-1}(\widetilde{\mathbf{x}} + \delta\widetilde{x}\,\mathbf{i}) - d^{-1}(\widetilde{\mathbf{x}} - \delta\widetilde{x}\,\mathbf{i})}{2\delta\widetilde{x}} \times \frac{d^{-1}(\widetilde{\mathbf{x}} + \delta\widetilde{y}\,\mathbf{j}) - d^{-1}(\widetilde{\mathbf{x}} - \delta\widetilde{y}\,\mathbf{j})}{2\delta\widetilde{y}} \right]. \tag{B.4}$$

This is the approximation used in the numerical experiments of this article.

References

Belo Pereira M, Berre L. 2006. The use of an ensemble approach to study the background-error covariances in a global NWP model. *Mon. Weather Rev.* **134**: 2466–2489.

Berre L, Pannekoucke O, Desroziers G, Stefanescu S, Chapnik B, Raynaud L. 2007. 'A variational assimilation ensemble and the spatial filtering of its error covariances: increase of sample size by local spatial averaging'. In *Proceedings of workshop on flow-dependent aspects of data assimilation*, 11–13 June 2007. 151–168. ECMWF: Reading, UK.

Bouttier F. 1993. The dynamics of error covariances in a barotropic model. *Tellus A* **45**: 408–423.

Bouttier F. 1994. A dynamical estimation of error covariances in an assimilation system. *Mon. Weather Rev.* **122**: 2376–2390.

Ciarlet P. 2006. *An introduction to differential geometry with application to elasticity*. Springer: Berlin.

Clerc M, Mallat S. 2002. The texture gradient equation for recovering shape from texture. *IEEE Trans. Pattern Anal. Machine Intell.* **24**: 536–549.

Cohn SE. 1993. Dynamics of short-term univariate forecast error covariances. *Mon. Weather Rev.* **121**: 3123–3149.

Courtier P, Andersson E, Heckley W, Pailleux J, Vasiljević D, Hamrud M, Hollingsworth A, Rabier F, Fisher M. 1998. The ECMWF implementation of three-dimensional variational assimilation (3D-Var). I: Formulation. *Q. J. R. Meteorol. Soc.* **124**: 1783–1807.

Daley R. 1991. *Atmospheric Data Analysis*. Cambridge University Press: Cambridge, UK.

Desroziers G. 1997. A coordinate change for data assimilation in spherical geometry of frontal structures. *Mon. Weather Rev.* **125**: 3030–3038.

Eells J, Sampson JH. 1964. Harmonic mappings of Riemannian manifolds. *Amer. J. Math.* **86**: 109–160.

Evensen G. 1994. Sequential data assimilation with a nonlinear quasi-geostrophic model using Monte Carlo methods to forecast error. *J. Geophys. Res.* **99**: 10143–10162.

Feynman RP, Morinigo F, Wagner W, Hatfield B, Pines D. 2002. *Feynman Lectures On Gravitation (Frontiers in Physics)*. Westview Press: Boulder, CO.

Fisher M. 2003. 'Background-error covariance modelling'. In *Proceedings of seminar on recent developments in data assimilation for atmosphere and ocean*. 45–63. ECMWF: Reading, UK.

Fisher M, Courtier P. 1995. 'Estimating the covariance matrices of analysis and forecast error in variational data assimilation'. Tech Memo 220. ECMWF: Reading, UK.

Gaspari G, Cohn S. 1999. Construction of correlation functions in two and three dimensions. *Q. J. R. Meteorol. Soc.* **125**: 723–757.

Greybush SJ, Kalnay E, Miyoshi T, Ide K, Hunt BR. 2011. Balance and Ensemble Kalman Filter localization techniques. *Mon. Weather Rev.* **139**: 511–522.

Houtekamer P, Mitchell H. 2001. A sequential ensemble Kalman filter for atmospheric data assimilation. *Mon. Weather Rev.* **129**: 123–137.

Kalman RE. 1960. A new approach to linear filtering and prediction problems. *J. Basic Eng.* **82**: 35–45.

Kepert J. 2009. Covariance localisation and balance in an Ensemble Kalman Filter. *Q. J. R. Meteorol. Soc.* **135**: 1157–1176.

Lyster PM, Cohn S, Zhang B, Chang L-P, Menard R, Olson K, Renka R. 2004. A Lagrangian trajectory filter for constituent data assimilation. *Q. J. R. Meteorol. Soc.* **130**: 2315–2334.

Massart S, Piacentini A, Pannekoucke O. 2012. Importance of using ensemble estimated background error covariances for the quality of atmospheric ozone analyses. *Q. J. R. Meteorol. Soc.* **138**: 889–905.

Menard R, Cohn S, Chang L-P, Lyster PM. 2000. Assimilation of stratospheric chemical tracer observations using a Kalman Filter. Part I: Formulation. *Mon. Weather Rev.* **128**: 2654–2671.

Michel Y. 2013a. Estimating deformations of random processes for correlation modelling in a limited-area model. *Q. J. R. Meteorol. Soc.* **139**: 534–547.

Michel Y. 2013b. Estimating deformations of random processes for correlation modelling: methodology and the one-dimensional case. *Q. J. R. Meteorol. Soc.* **139**: 771–783.

Nakahara M. 2003. *Geometry, Topology and Physics* (2nd ed.) Taylor & Francis: Abingdon, UK.

Pannekoucke O. 2009. Heterogeneous correlation modeling based on the wavelet diagonal assumption and on the diffusion operator. *Mon. Weather Rev.* **137**: 2995–3012.

Pannekoucke O, Massart S. 2008. Estimation of the local diffusion tensor and normalization for heterogeneous correlation modelling using a diffusion equation. *Q. J. R. Meteorol. Soc.* **134**: 1425–1438.

Pannekoucke O, Berre L, Desroziers G. 2008. Background-error correlation length-scale estimates and their sampling statistics. *Q. J. R. Meteorol. Soc.* **134**: 497–508.

Purser RJ, Wu W-S, Parrish D, Roberts N. 2003. Numerical aspects of the application of recursive filters to variational statistical analysis. Part I: Spatially homogeneous and isotropic Gaussian covariances. *Mon. Weather Rev.* **131**: 1524–1535.

Raynaud L, Pannekoucke O. 2013. Sampling properties and spatial filtering of ensemble background-error length-scales. *Q. J. R. Meteorol. Soc.* **139**: 784–794.

Raynaud L, Berre L, Desroziers G. 2009. Objective filtering of ensemble-based background-error variances. *Q. J. R. Meteorol. Soc.* **135**: 1177–1199.

Smolarkiewicz P, Margolin LG. 1994. Variational solver for elliptic problems in atmospheric flow. *Appl. Math. Comp. Sci.* **4**: 527–551.

Weaver AP, Courtier P. 2001. Correlation modelling on the sphere using a generalized diffusion equation. *Q. J. R. Meteorol. Soc.* **127**: 1815–1846.

Zdunkowski W, Bott A. 2003. *Dynamics of the Atmosphere: A Course in Theoretical Meteorology*. Cambridge University Press, Cambridge, UK.

